Air Gap Fiber Fabry–Pérot Interferometer for Highly Sensitive Micro-Airflow Sensing

Cheng-Ling Lee, *Member, IEEE*, Wan-Yu Hong, Hsin-Jung Hsieh, and Zi-Yu Weng

***Abstract*—This work presents a novel sensor based on an air-gap fiber Fabry–Pérot interferometer (AG-FFPI) to identify an extremely low airflow velocity. When a micro airflow flows through the upper side of the sensor, an extremely small pressure difference caused by fluid mechanics makes two fiber endfaces tilt upwards and generates a tiny discrepancy between the two aligned fiber endfaces. This discrepancy of the AG-FFPI changes the air gap, and the center wavelength of the specific interference dips. The proposed sensor can determine the velocity of a micro airflow from a surrounding environment within 0 $\sim$ 1.2 m/s. In addition, the wavelength of shifts in interference fringes is nearly proportional to airflow velocity with a high sensitivity of approximately $+33.17\ \mathrm{nm}/(\mathrm{m}\cdot\mathrm{s}^{-1})$.**

***Index Terms*—Airflow, air-gaps, Fabry–Pérot interferometer, fiber-optics component, fiber sensors.**

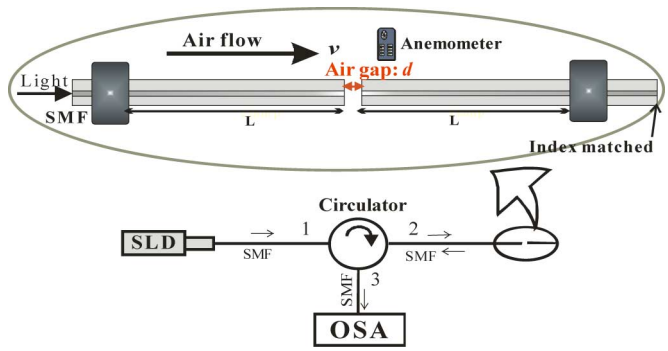

Fig. 1. Configuration of the air-gap fiber Fabry–Pérot interferometer (AG-FFPI).

I. Introduction

AMONG the various applications the airflow detection plays an important role in mechanical, electronic, biotechnology, chemical and medical applications. Measurement principles are based on mechanical [1], [2] and electronic systems [3] microelectromechanical systems (MEMSs) [4]–[6] and fiber-optics schemes [7]–[10]. Especially, in [7], light input in an etched thinned fiber-tip cantilever reduced optical coupling to a receiving multimode fiber when the fluidic drag force acts on the fiber-tip to shift the emitting light from the fiber. The above sensor alignment must be guided by a designed microfluidic channel, and fabricated by a chemical etched process. Another fiber-based sensor for fluid sensing based on the well known optical fiber Bragg grating (FBG) [8], [9] is sensitive with nonelectrical operation. A situation in which the force created by the fluid affects the FBGs causes their bending or distortion with the strain acting. Although FBG based device is effective, proper fabricating techniques are required and the measured mechanism requires temperature compensation since the FBG is highly sensitive to the ambient temperature. Wehrmeister *et al.* [10] developed a Fabry–Pérot interferometer based on the fiber-optical cables integrated precisely in a microchip to detect gas and liquid from the interference signals. Above sensors are useful, yet require complex and integrated fabrication for sensing the fluid or pressure.

Manuscript received January 28, 2011; revised April 01, 2011; accepted April 09, 2011. Date of publication April 15, 2011; date of current version June 08, 2011. This work was supported in part by the National Science Council of the Republic of China under Grant NSC 98-2221-E-239-002-MY2.

The authors are with the Department of Electro-Optical Engineering, National United University, Miaoli 360, Taiwan (e-mail: cherry@nuu.edu.tw).

Color versions of one or more of the figures in this letter are available online at http://ieeexplore.ieee.org.

Digital Object Identifier 10.1109/LPT.2011.2142413

This work presents a novel and simple optical sensor that determines weak airflows accurately and efficiently. The proposed ultrasensitive AG-FFPI airflow sensor can detect airflow velocity with very weak variations around the surrounding environment by measuring the wavelength shifts of interference fringe. Experimental results demonstrate that wavelengths of the interference fringe shift are almost proportional to the velocity with 0 $\sim$ 1.2 m/s of a microflow with a highly sensitive resolution.

II. Sensor Configuration and Principle of Operation

The proposed AG-FFPI contains two arranged single-mode fibers (SMFs) separated by a small air gap with a certain length of d (Fig. 1). Our previous study obtained an unsatisfactory sensitivity when the used fibers were still with the jacket [11]. This work attempts to improve the sensitivity, in which two bare SMFs with an entire removal of the coating and well-cleaved endface are aligned precisely by using the fiber holder in optical stages. Two clamps fix the endface of both fibers with a blank section of length (L: fiber arm) and expose the top surface of the fibers to allow the micro airflow. A commercial anemometer with a resolution of 0.05 m/s was placed on the top of the sensor to monitor the steady airflow and indicate the airflow velocity. When micro airflow flows through the upper side of the sensor, an extremely small pressure difference caused by fluid mechanics causes two fiber endfaces to tilt up and make a vertical and horizontal displacements of air gap between the two aligned fiber endfaces, as shown in Fig. 2.

This tiny bending of fiber endface generates a very small change of the air gap (Δd), which changes the center wavelength of the specific interference dips. The small pressure difference (ΔP) can be elucidated by the well-known Bernoulli principle. In fluid dynamics applications, Bernoulli's principle

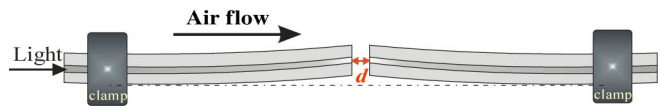

Fig. 2. Diagram of fiber endfaces tilt up when a micro airflow flows through upper side of the proposed sensor.

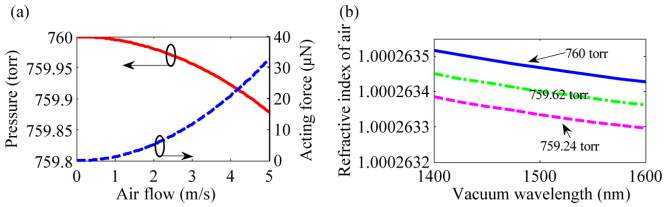

Fig. 3. (a) Curves for the relationship between pressure and airflow velocity based on Bernoulli's equation (solid line) and calculated acting force on the fiber tip (dashed line). (b) Refractive index of the air under different pressures.

states that for an inviscid flow, the fluid speed increases simultaneously with a decrease in pressure. Bernoulli's principle can thus be applied to airflows using the following simple form:

$$P + 1/2\rho v^2 = P_o \tag{1}$$

where P_o is a constant called total pressure, which equals 1 atmosphere (atm) $= 760$ torr $= 101325$ Pa (Pa $=$ N/m^2); v (m/s) is airflow velocity; ρ is air density, which is about 1.3 kg/m^3 at room temperature; P is surrounding pressure; and $1/2\rho v^2$ is dynamic pressure owing to v [12]. Fig. 3(a) plots the curves to describe the relationship between P and v based on Bernoulli's equation and the corresponding acting force (F) caused by the pressure difference $(\Delta P = P_o - P)$ when air flows. Notably, F is estimated by $F = \Delta P \times A$, where $A = 2aL$ represents the cross-sectional area of the cylindrical fiber arm (cladding radius a). The curve reveals that pressure (P) decreases when airflow increases and F increases with a rising airflow velocity. To further elucidate the optical properties of air related pressure, Fig. 3(b) displays the refractive index (n) dispersion profiles of air for various atmospheric pressures at 25°C. Variation in the n related to pressure change for the air is extremely small at roughly 10^{-7}/torr. Thus, the interference fringe shift caused by refractive index variation of the air can be ignored.

III. Results and Discussion

Operations of the proposed AG-FFPI sensor for various airflow velocities are investigated by using samples with air gaps of $d = 20$, 30, and 40 μm to measure extremely weak airflows. Fig. 4(a) shows the interference fringes shift to long wavelengths as airflow velocity increases with the $d = 20$ μm and $L = 1.2$ cm. Inset in Fig. 4(a) shows the corresponding central wavelength shifts for a dip around 1550 nm. The Fig. 4(a) shows $d = 20$ μm since the results of the other air gaps have the same sinusoidal curve spectra. Fig. 4(b) plots the corresponding sensitivity and tuning efficiency. The best sensitive efficiency is estimated at about $+33.17$ nm/(m $\cdot$ s^{-1}) with $d = 20$ μm. The characteristics of the AG-FFPI can be modeled using the two-beam optical interference theorem. For an intensity-based interferometer, the visibility of the interference fringes depends on the intensity of the two beams, and the equivalent intensities of the two beams determine the best interference performance

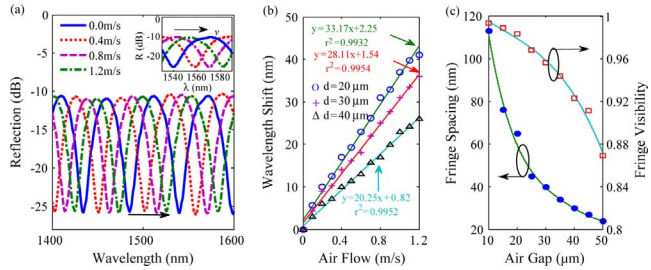

Fig. 4. (a) Reflection spectra of the proposed sensor with different air flow velocities ($v = 0 \sim 1.2$ m/s) for the $d = 20$ μm and $L = 1.2$ cm. (b) Airflow sensitivity of shifts in the interference peaks with different d. (c) Average fringe spacing and fringe visibility as a function of d at $v = 0$ m/s.

and maximum fringe visibility. Thus, these two beams are defined as the Fresnel reflections by the first and second fiber/air interfaces: I_1, and I_2, respectively. The optical phase difference between the two beams $\Phi = (2\pi/\lambda) \cdot (\text{OPD})$, where OPD $= 2d$ is the optical path difference. Therefore, the reflected intensity in interference fringes can be easily expressed:

$$I_{\text{int}} = I_1 + I_2 + 2\sqrt{I_1 I_2}\cos(\Phi) \tag{2}$$

The mth interference fringe spacing $\Delta\lambda$ is estimated to be $\Delta\lambda \sim \lambda_m \lambda_{m+1}/(\text{OPD})$, with $\Delta\lambda \cong \lambda_{m+1} - \lambda_m$, m an integer and λ_m and λ_{m+1} the central wavelengths of the two valleys adjacent to the mth valley in the spectrum. The two adjacent interference minimums have a phase difference of 2π. Variation of the air gap $(\Delta d = d' - d)$ and wavelength shift $(\Delta\lambda_m)$ of the m^{th} center wavelength dip of the specific interference fringe with the following relation :

$$\frac{\Delta d}{d} = \frac{\Delta\lambda_m}{\lambda_m} \tag{3}$$

where λ_m is the m^{th} center wavelength dip. According to (3), smaller air gap d has a larger $\Delta\lambda_m$ at the same airflow. The ratio of the $\Delta d/d$ decides the wavelength dips shift. This means the shorter air gap distance has smaller tolerance of the alignment for two fibers. Estimations are in good agreement with experimental results which are shown in Fig. 4(b) since a poor sensitivity of the measured result is obtained when the d increases. The average fringe spacing and fringe visibility as a function of the d are shown in Fig. 4(c) at wavelength around 1550 nm. The fringe spacing in this type of interferometers decreases exponentially with the d increasing (dot). As the interference visibility (square) also decreases smoothly with the d since longer d to the fact that light travels longer that the reflection beam I_2 becomes weaker so that makes a poor interference patterns.

Fig. 5 illustrates a diagram of the tilted fiber end with different d at the same air flow. Smaller d (case1) has a larger deviation angle (θ) and a stronger change than those of case2 when vertical displacement s is the same (same F on the same L, i.e. the same tilted situation). Because s, Δd and θ are all very small, from the geometric structure of Fig. 5, the Δd (equivalently horizontal displacement) is approximately expressed as below:

$$\Delta d \sim d' - d \sim 2s\theta \sim 4s^2/d. \tag{4}$$

In Fig. 5, the angle $\theta_1 > \theta_2$ corresponds to the variation $\Delta d_1 > \Delta d_2$. Thus, again from (4), a smaller d has a greater

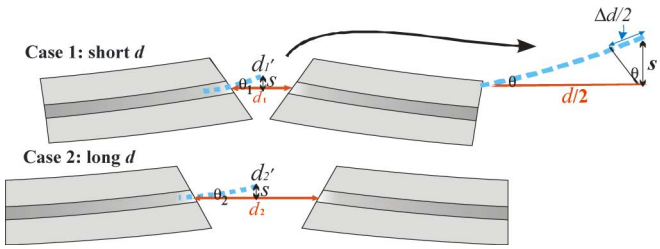

Fig. 5. Diagrams of the tilted fiber tip with different d at the same airflow; here d and d' are the effective air-gaps before and after air flowing, respectively.

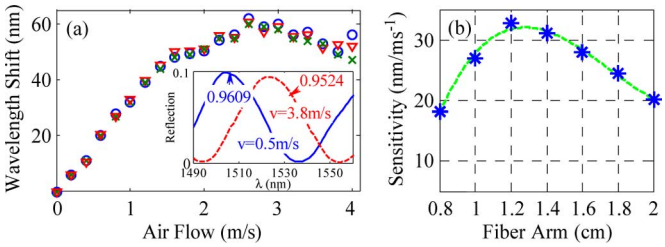

Fig. 6. (a) Wavelength shifts ($\Delta\lambda_m$) with the airflow $v = 0 \sim 4$ m/s measured by the sensor. (b) Measured sensitivity with different fiber arm (L) of the device in linear response condition $v = 0 \sim 1.2$ m/s.

Δd, implying that a larger wavelength shift $\Delta\lambda_m$ can be achieved, i.e. enhanced sensor sensitivity. Here, although vertical displacement s depends on the effective force acting on the fiber tip, the fiber is not a rigid rod and with elasticity. Therefore, the fiber bending caused by the torque applied on the fiber tip may have nonlinearity and the s of the fiber tip is difficult to estimate. However, with the measured results of Fig. 4(a) and (3) and (4), Δd can be calculated as 0.428 μm with $v = 1$ m/s, $\lambda_m = 1550$ nm, $d = 20$ μm, $L = 1.2$ cm, and $\Delta\lambda_m = 33.17$ nm. Thus, the s can be readily estimated at around 1.4628 μm. The tilted height, s is quite small since the calculated acting force F on the fiber tip is only about 1.3 μN (Fig. 3(a)) at the air flow of 1 m/s. To further investigate the sensing properties of the proposed sensor in a high airflow and different length of fiber arms, Fig. 6 shows the experimental results. In Fig. 6(a), the $\Delta\lambda_m$ value with a flow velocity from $v = 0 \sim 4$ m/s, $d = 20$ μm, $L = 1.2$ cm conditions is recorded for many repeated measurements. According to this figure, the sensor presents an excellent linearity response and stable results when the measured range is $v = 0 \sim 1.2$ m/s. However; a nonlinear sensitivity and rather unstable results are obtained when in a high airflow. Inset shows fringe visibility is reduced when at high airflow.

Experimental results indicate that a high v has larger $\Delta\lambda_m$, but with nonlinearity response, a little lower fringe visibility and an unstable response. This is because the fiber tip may vibrate by turbulence and has nonlinear dynamics when a higher torque acts on the bigger bending of the elastic rod. As the fiber arm L affects the sensing performance of the device, the vertical displacement s for stiffness is approximately modeled as [7]:

$$s \propto \frac{FL^3}{Ea^4} \tag{5}$$

Where F is the net force acting against the fiber tip, and E represents the Young's modulus of silica fiber. Although (5) is not representing real situation for our device, it indicates that the sensitivity increases with an increasing L and a decreasing a. However, too long of the L (i.e. too heavy) reduces the net force and degrades the sensitivity as illustrated in Fig. 6(b). In our design, a best sensitivity can be found when L is around 1.2 cm with the $d = 20$ μm; in addition, the airflow is under a linear sensitive range $v = 0 \sim 1.2$ m/s. The condition at a longer L is unstable and much heavier that influences the fiber tip tilted up. Moreover, a short L implies a rigid rod property that lacks elasticity, possibly reducing the tilted and bending capability and subsequently causing an unsatisfactory sensitive capability.

IV. Conclusion

This work demonstrates the feasibility of a highly sensitive microfluidic sensor for small airflows based on an AG-FFPI device. Based on Bernoulli's principle, the pressure difference caused by air flowing through one side of the sensor causes two fiber endfaces to tilt up and make a slight alignment deviation. Doing so causes a shift in the center wavelength of optical interference dips. Experimental results indicate that the wavelengths fringes shift are well proportional to weak airflow with a high sensitivity. The optimal length of the fiber arm L is at around 1.2 cm in the proposed configuration. We believe that the proposed device is a highly attractive sensor with many potential applications in microfluidic or hydrobiological sensing.

References

[1] J. S. J. Chen, "On the design of a wide range mini-flow paddlewheel flow sensor," *Sens. Actuator A, Phys.*, vol. 87, pp. 1–10, 2000.
[2] M. Dijkstra, J. J. van. Baar, R. J. Wiegerink, T. S. J. Lammerink, J. H. ve. Boer, and G. J. M. Krijnen, "Artificial sensory hairs based on the flow sensitive receptor hairs of crickets," *J. Micromech. Microeng.*, vol. 15, p. S132, 2005.
[3] A. Poghossian, T. Yoshinobu, and M. J. Schöning, "Flow-velocity microsensors based on semiconductor field effect structures," *Sensors*, vol. 3, pp. 202–212, 2003.
[4] S. Kim, T. Nam, and S. Park, "Measurement of flow direction and velocity using a micromachined flow sensor," *Sens. Actuators A, Phys.*, vol. 114, pp. 312–318, 2004.
[5] S. Park, S. Kim, S. Kim, and Y. Kim, "A flow direction sensor fabricated using MEMS technology and its simple interface circuit," *Sens. Actuators B, Chem.*, vol. 91, pp. 347–352, 2003.
[6] Y. H. Wang, C. Y. Lee, and C. M. Chiang, "A MEMS-based air flow sensor with a free-standing microcantilever structure," *Sensors*, vol. 7, pp. 2389–2401, 2007.
[7] V. Lien and F. Vollmer, "Microfluidic flow rate detection based on integrated optical fiber cantilever," *Lab Chip*, vol. 7, pp. 1352–1356, 2007.
[8] J. Lim, Q. P. Yang, B. E. Jones, and P. R. Jackson, "DP flow sensor using optical fibre Bragg grating," *Sens. Actuator A, Phys.*, vol. 92, pp. 102–108, 2001.
[9] Y. Zhao, K. Chen, and J. Yang, "Novel target type flowmeter based on a differential fiber Bragg grating sensor," *Measurement*, vol. 38, pp. 230–235, 2005.
[10] J. Wehrmeister, A. Fuss, F. Saurenbach, R. Berger, and M. Helm, "Readout of micromechanical cantilever sensorarrays by Fabry–Perot interferometry," *Rev. Sci. Instrum.*, vol. 78, p. 104105(1-9), 2007.
[11] W.-Y. Hong, Z.-Y. Weng, C.-M. Li, H.-J. Hsieh, F.-C. Hu, and C.-L. Lee, "Air-gap Fabry-Perot fiber interferometer for highly sensitive air flow sensing," *Opt. Photo. Taiwan*, p. OPT5-P-006, 2010.
[12] G. A. Lindsay, "Pressure energy and Bernoulli's principle," *Amer. J. Phys.*, vol. 20, pp. 86–88, 1952.